Irfu
Institute of Research
into the Fundamental Laws of the Universe

Reconstruction and denoising of dark matter map based on Multigrid Method from weak lensing data

14/11/2014

Ming JIANG (Cosmostat/Irfu)

Tutors:
Jean-Luc Starck (AIM, CEA Saclay)
Erwan Deriaz (Université de Lorraine)

Outline

- **Context**
- **Dark matter map reconstruction**
- **Dark matter map denoising**
- **Conclusions**

Cosmology model

- **Universe content: “Dark” Universe**

  Visible matter represent only about 5% of the Universe

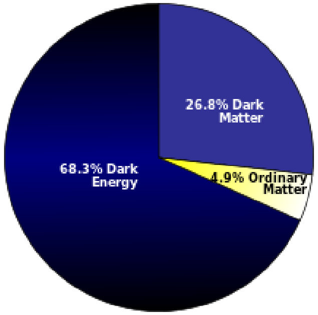

- **Weak lensing**

  The most promising tool to understand the nature of dark matter

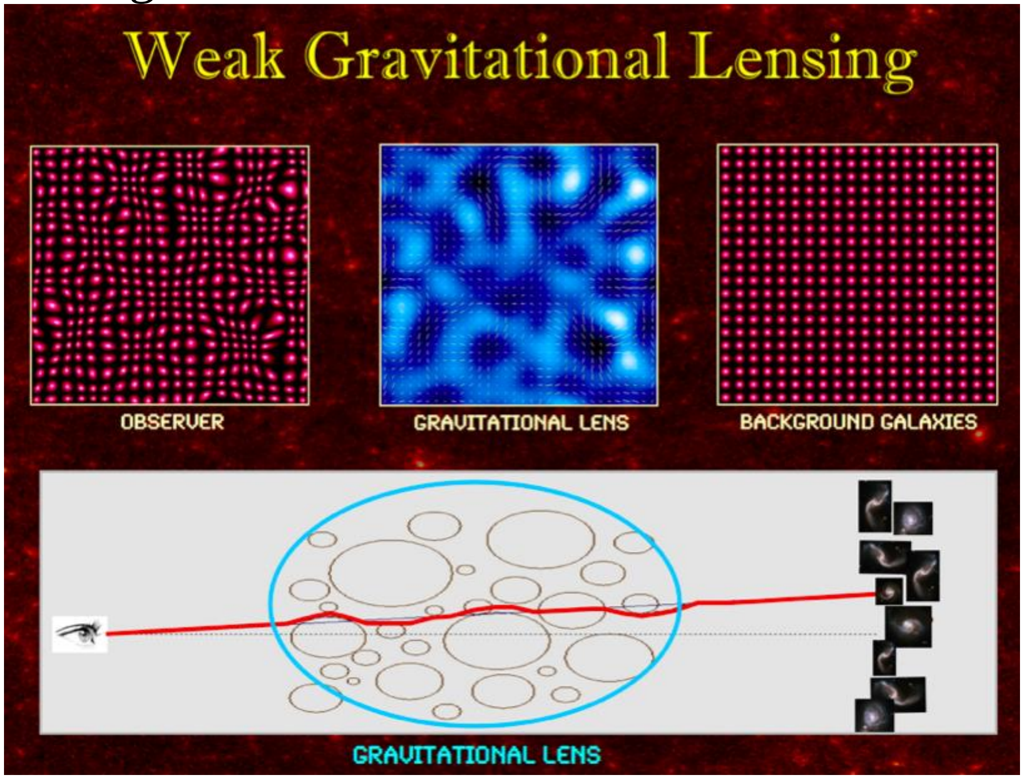

Weak lensing

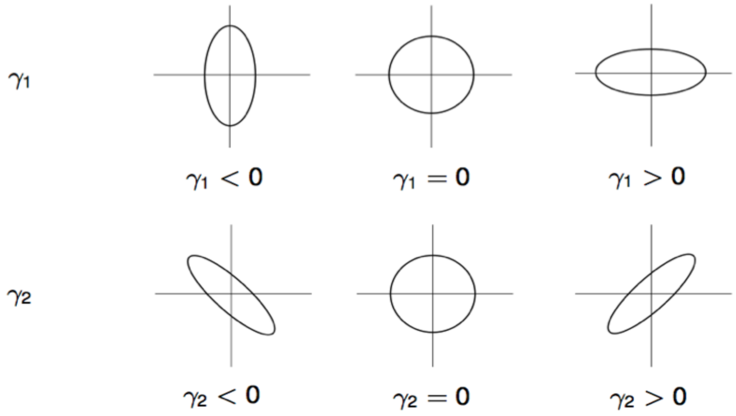

- **The shear map $\gamma(\gamma_1, \gamma_2)$**

γ_1 = deformation in horizontal direction

γ_2 = deformation in diagonal direction

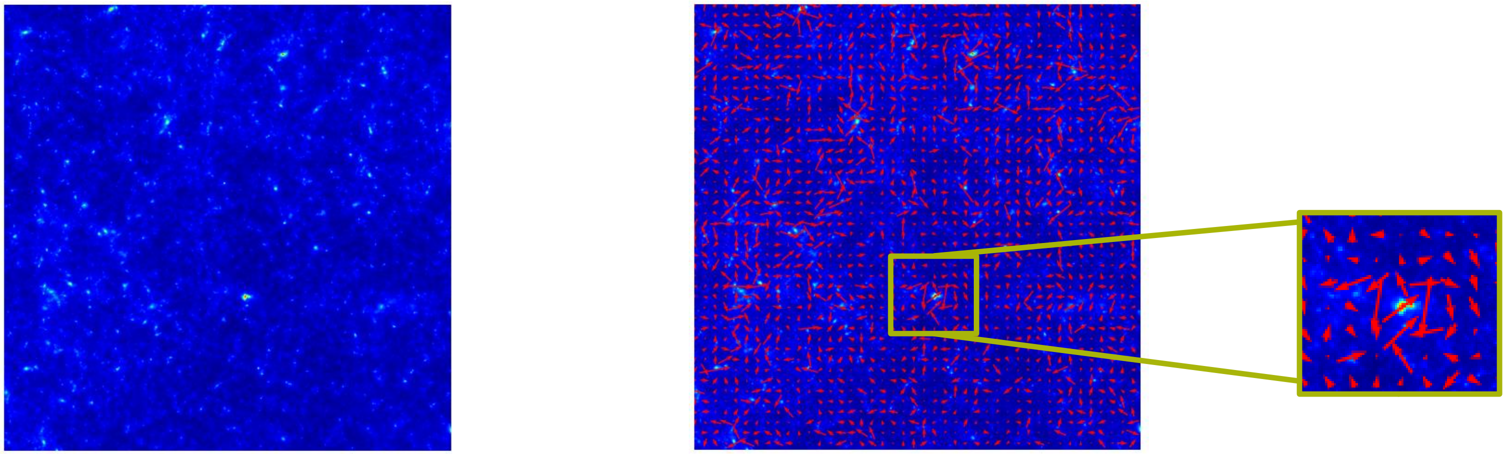

(a) (b)

Figure: (a)The simulated convergence map κ, (b)The shear map γ is superimposed to the convergence map κ.

Dark matter map reconstruction

Inverse problem

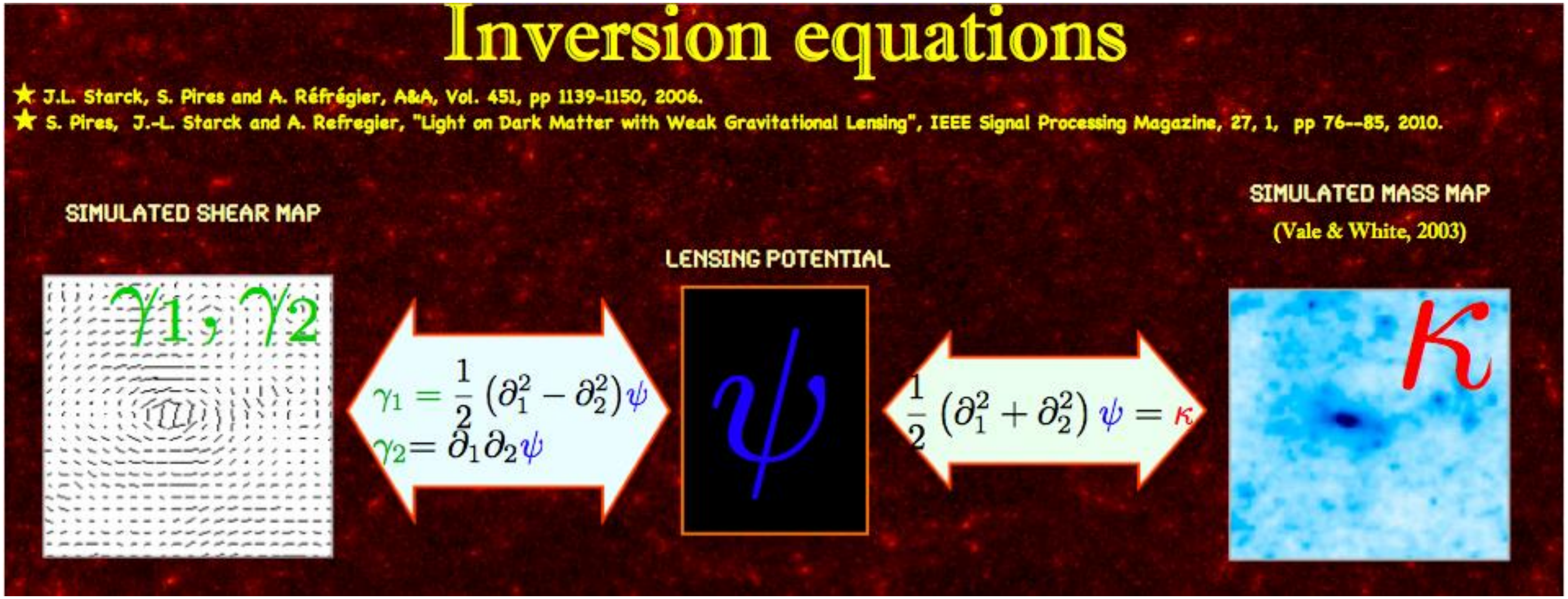

- **E and B modes decomposition** .

  We use a field u *(Deriaz, Pires, Starck; A&A; 2012)* such that

$$u = \nabla \kappa_E + \nabla \times \kappa_B \quad \text{with} \quad u = \begin{bmatrix} -\gamma_{1,1} - \gamma_{2,2} \\ -\gamma_{2,1} + \gamma_{1,2} \end{bmatrix}$$

Because the weak lensing arises from a scalar potential, it can be shown that weak lensing only produces E modes to the first order.

Solutions

- Fourier Transform: remove the partial differential, boundary effects
- **New solution:**

$$\boldsymbol{\Delta\kappa_B} = \left(-\boldsymbol{\partial_1^2} + \boldsymbol{\partial_2^2}\right)\boldsymbol{\gamma_1} + \boldsymbol{2\partial_1\partial_2\gamma_2} \qquad (1)$$

$$\boldsymbol{\Delta\kappa_E} = \left(\boldsymbol{\partial_1^2} - \boldsymbol{\partial_2^2}\right)\boldsymbol{\gamma_1} + \boldsymbol{2\partial_1\partial_2\gamma_2} \qquad (2)$$

1. Reconstruct B modes according to the Poisson equation (1) and the boundary condition $\kappa_B = 0$
2. Obtain the Dirichlet boundary condition for E modes by the line integration

$$\kappa_E = \oint_{\Gamma} (\boldsymbol{u} - \boldsymbol{\nabla} \times \boldsymbol{\kappa_B}) \cdot d\boldsymbol{s}$$

3. Reconstruct E modes according to the Poisson equation (2) and the boundary condition obtained in the previous step.

- **Techniques: Multigrid (MG), Finite Difference method (FDM).**

Discretization

- **As for a Poisson equation Δf = g**

$$f_{i+1,j} + f_{i-1,j} + f_{i,j+1} + f_{i,j-1} - 4f_{i,j} = h^2 g_{i,j}$$

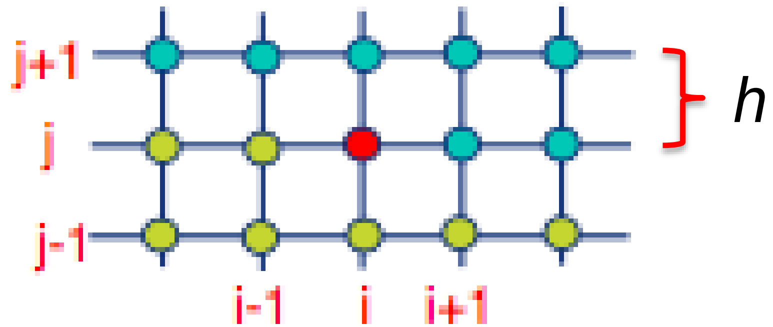

- **Elementary iterative methods:**

Rate of convergence: Very long!!!

$$f^{n+1}{}_{i,j} = \frac{1}{4}\left[f^{n}{}_{i+1,j} + f^{n}{}_{i-1,j} + f^{n}{}_{i,j+1} + f^{n}{}_{i,j-1} - h^2 g_{i,j}\right] \quad \textbf{Jacobi}$$

$$f^{n+1}{}_{i,j} = \frac{1}{4}\left[f^{n}{}_{i+1,j} + f^{n+1}{}_{i-1,j} + f^{n}{}_{i,j+1} + f^{n+1}{}_{i,j-1} - h^2 g_{i,j}\right] \quad \textbf{Gauss-Seidel}$$

$$f^{n+1}{}_{i,j} = \frac{\beta}{4}\left[f^{n}{}_{i+1,j} + f^{n+1}{}_{i-1,j} + f^{n}{}_{i,j+1} + f^{n+1}{}_{i,j-1} - h^2 g_{i,j}\right] + (1-\beta) f^{n}_{i,j} \quad \textbf{SOR}$$

Why use the MG?

- **Why Elementary iterative methods are not efficient?**

  Local processing, but not global processing.

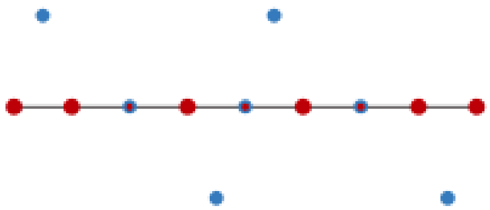

Blue point: previous position
Red point: current position

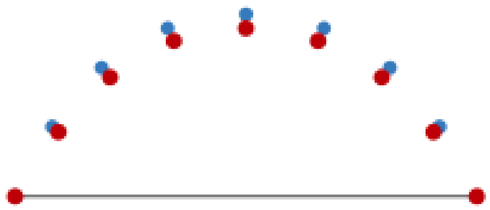

- **Multigrid method:**

  Global processing, to eliminate large-scale error on the coarser grid

$$\boldsymbol{A(f_{app}+e)=g} \longleftrightarrow \boldsymbol{Ae=g-Af_{app}=r}$$

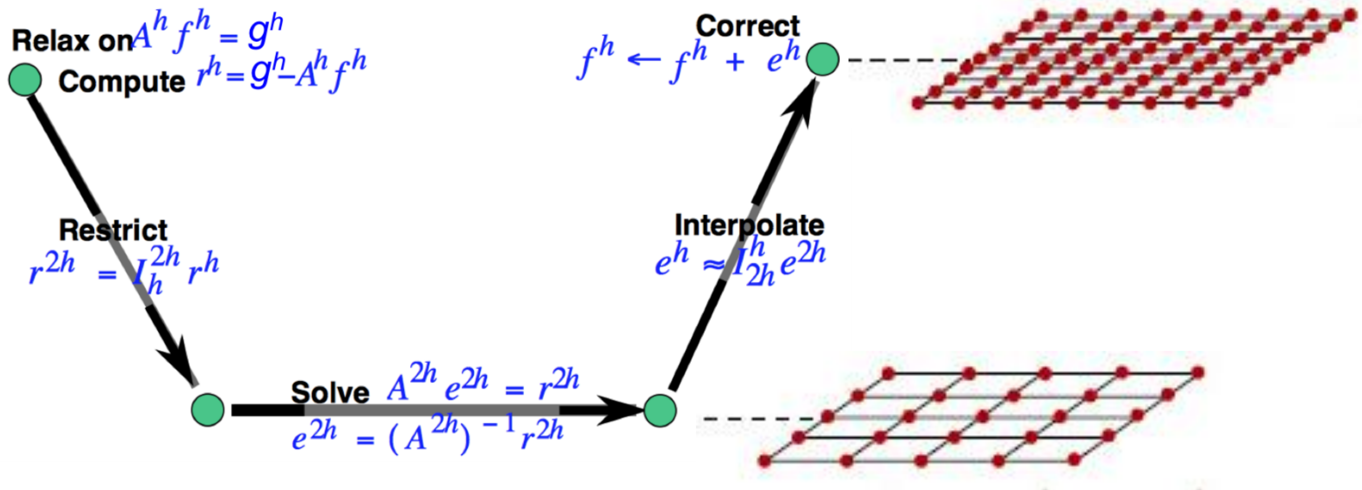

MG V-Cycle

- How do we "solve" the coarse- grid residual equation? **Recursion**
- V-Cycle

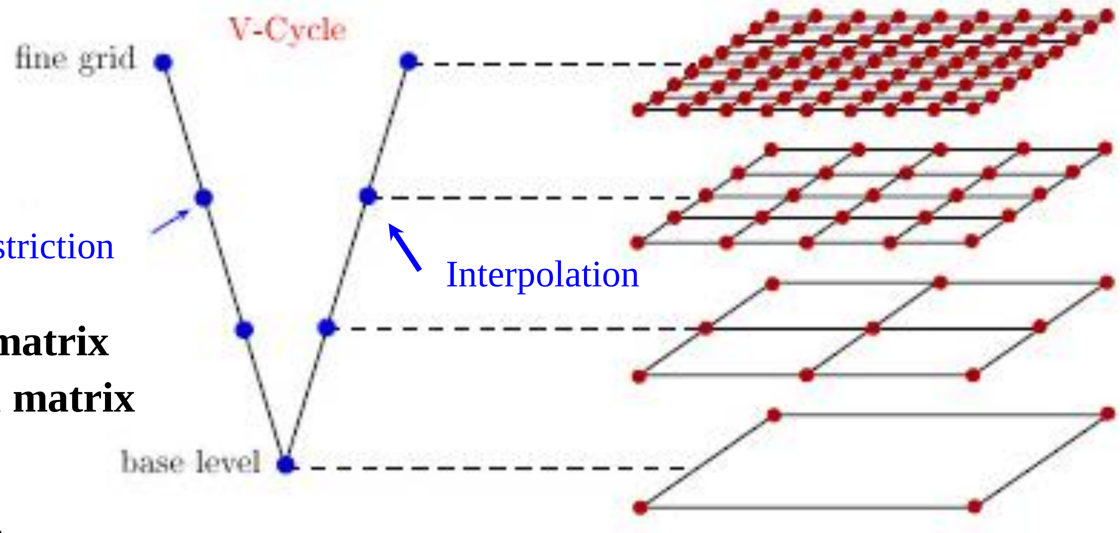

***R* = R_h^{2h} = restriction matrix**

***I* = I_{2h}^{h} = interpolation matrix**

- Algorithm

1. **Iterate** on $A_h f = g_h$ to reach f_h (say 3 Jacobi or Gauss-Seidel steps).
2. **Restrict** the residual $r_h = g_h - A_h f_h$ to the coarse grid by $r_{2h} = R_h^{2h} r_h$.
3. **Solve** $A_{2h} E_{2h} = r_{2h}$ (or come close to E_{2h} by 3 iterations from $E = 0$).
4. **Interpolate** E_{2h} back to $E_h = I_{2h}^h E_{2h}$. Add E_h to f_h.
5. **Iterate** 3 more times on $A_h f = g_h$ starting from the improved $f_h + E_h$.

Numerical results

- **MG**

$$\frac{\left\|\tilde{\kappa}_E - \kappa\right\|_2}{\left\|\kappa\right\|_2} = 4.7\%$$

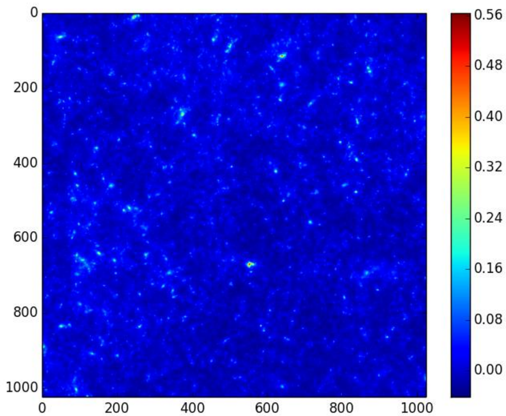

-

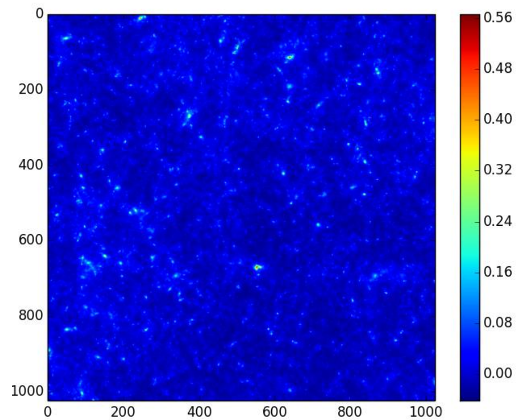

=

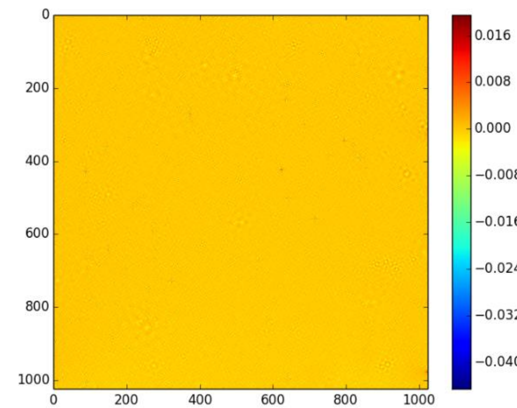

Reconstruction $\tilde{\kappa}_E$ | Original κ | Relative Errors

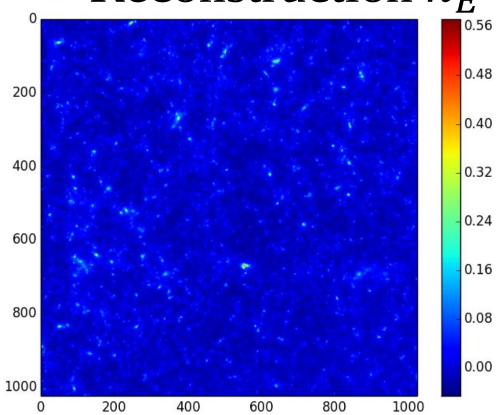

-

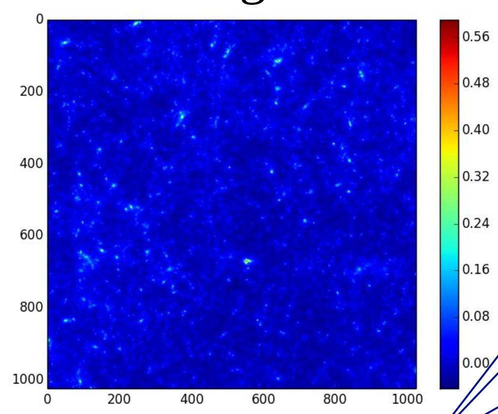

=

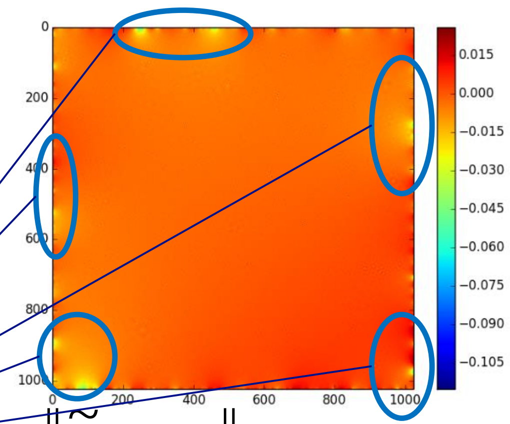

- **FFT**

Boundary effect !

$$\frac{\left\|\tilde{\kappa}_E - \kappa\right\|_2}{\left\|\kappa\right\|_2} = 20.1\%$$

Analysis of convergence

- **Complexity**

If error tolerance $\epsilon = Ch^2 \rightarrow$ V-Cycle times: $\mathcal{O}(\log N) \rightarrow$ global complexity: $\mathcal{O}(N^2 \log N)$
Further, $\epsilon = constant \rightarrow$ V-Cycle times: $constant \rightarrow$ global complexity: $\mathcal{O}(N^2)$

Very efficient !

Table : V-Cycles of MG (Stopping criteria: 10^{-4} between iterations)

Finest grid ($N \times N$)	V-Cycles for B modes	V-Cycles for E modes	Relative error
32×32	5	5	6.2%
64×64	5	7	4.1%
128×128	5	7	4.0%
256×256	6	7	4.5%
512×512	6	9	4.6%
1024×1024	7	8	4.7%

Irregular domain

■ Why should apply to the irregular domain?

In practice some areas of the survey of the telescope are masked because of foreground stars, this leads to a requirement of a proper handling of a complex geometry of the survey and of missing data.

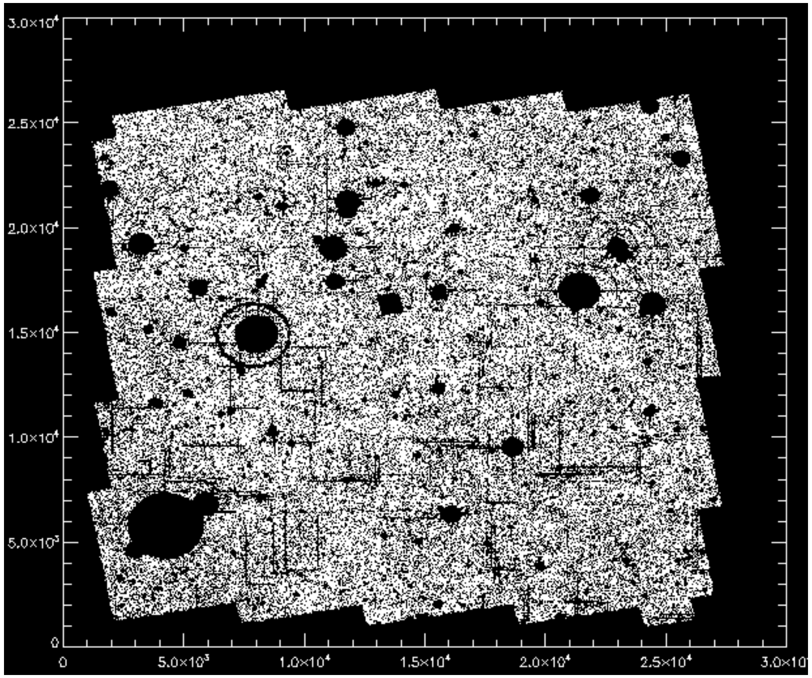

Figure : Plot of the COSMOS survey, each point represents a galaxy

Modeling

- **Examples**

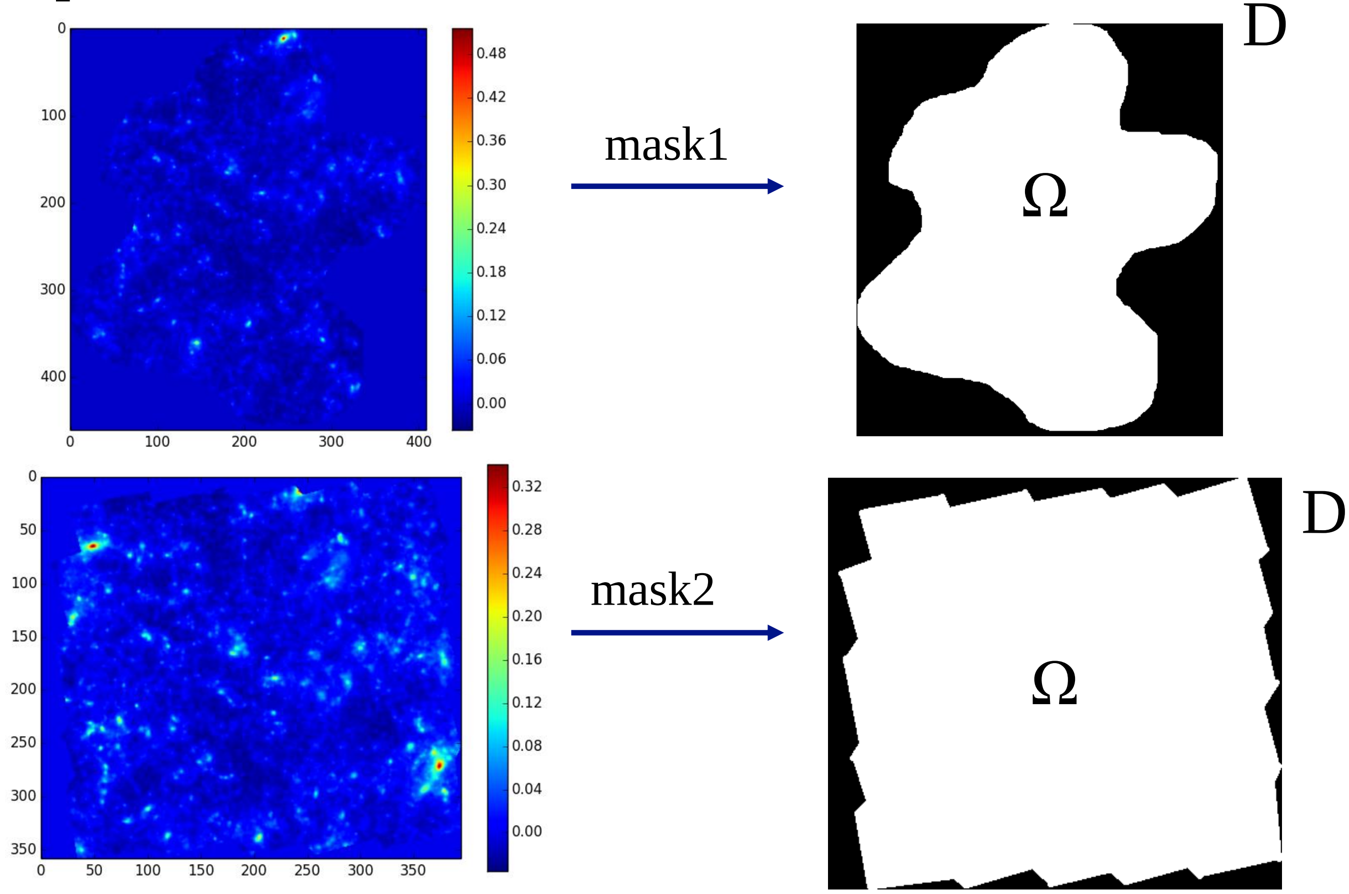

FDM for the complex geometry

FDM

A numerical method for approximating the solutions to differential equations using finite difference equations to approximate derivatives

- **Computation models**

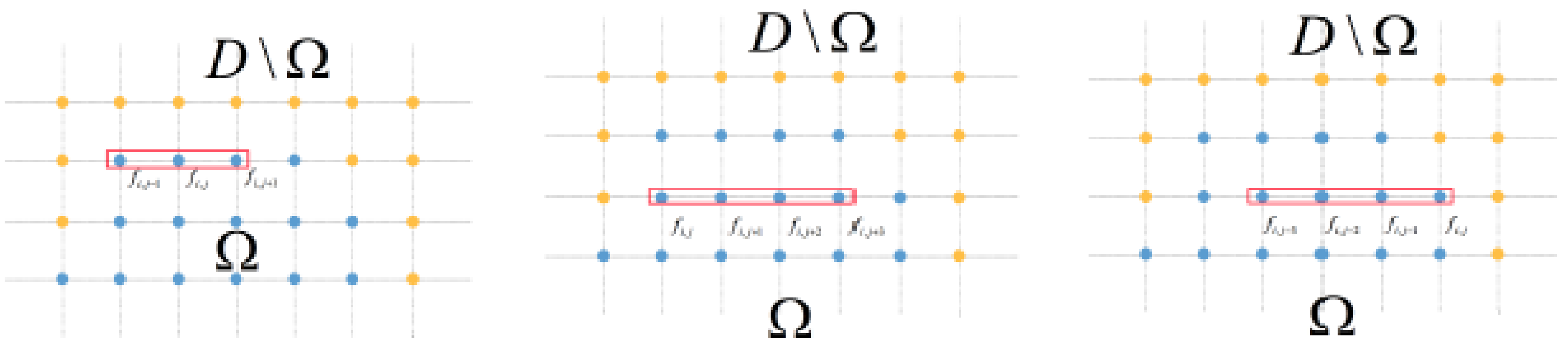

(a) Model 1 (b) Model 2 (c) Model 3

$$f'_{i,j} \approx \frac{-f_{i,j-1} + f_{i,j+1}}{2h} \qquad f'_{i,j} \approx \frac{-3f_{i,j} + 4f_{i,j+1} - f_{i,j+2}}{2h} \qquad f'_{i,j} \approx \frac{3f_{i,j-2} - 4f_{i,j-1} + f_{i,j}}{2h}$$

$$f''_{i,j} \approx \frac{f_{i,j-1} - 2f_{i,j} + f_{i,j+1}}{h^2} \qquad f''_{i,j} \approx \frac{4f_{i,j} - 5f_{i,j+1} + 4f_{i,j+2} - f_{i,j+3}}{h^2} \qquad f''_{i,j} \approx \frac{4f_{i,j-3} - 5f_{i,j-2} + 4f_{i,j-1} - f_{i,j}}{h^2}$$

Numerical results (irregular domain)

$$\frac{\left\|\tilde{\kappa}_E - \kappa\right\|_2}{\left\|\kappa\right\|_2} = 11.4\%$$

- **Mask1**

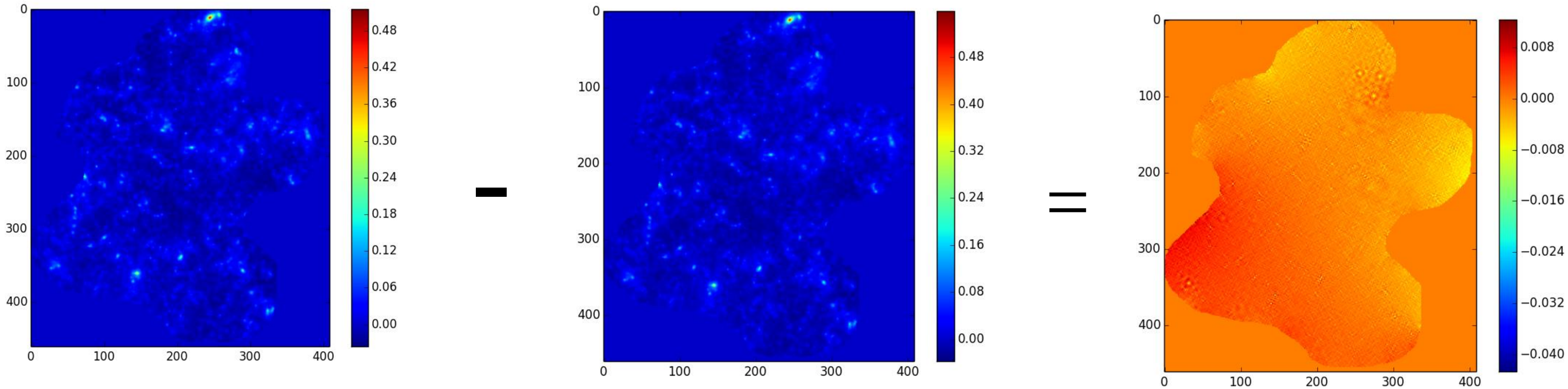

Reconstruction $\tilde{\kappa}_E$ Original κ Relative Errors

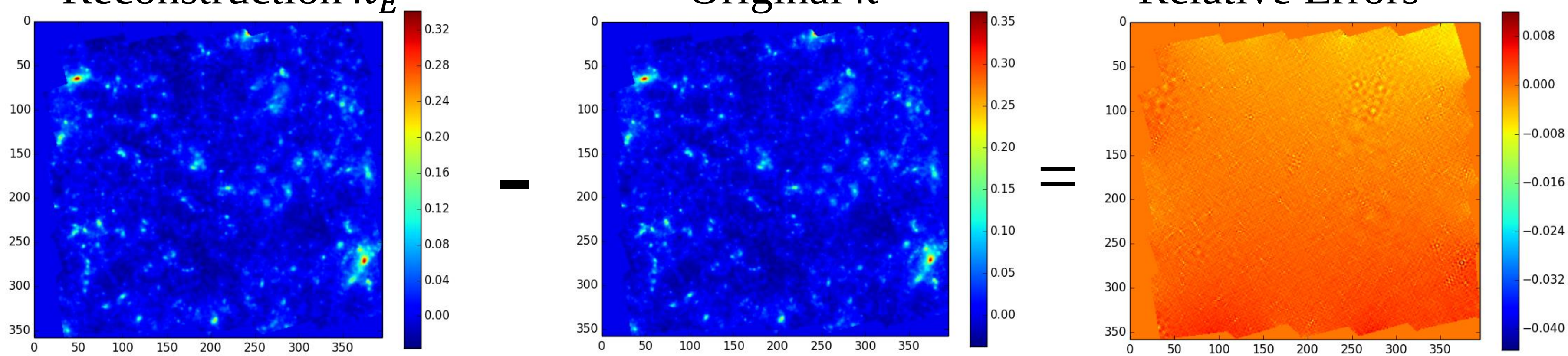

$$\frac{\left\|\tilde{\kappa}_E - \kappa\right\|_2}{\left\|\kappa\right\|_2} = 9.8\%$$

- **Mask2**

Irregular domain with "holes"

- **Example**

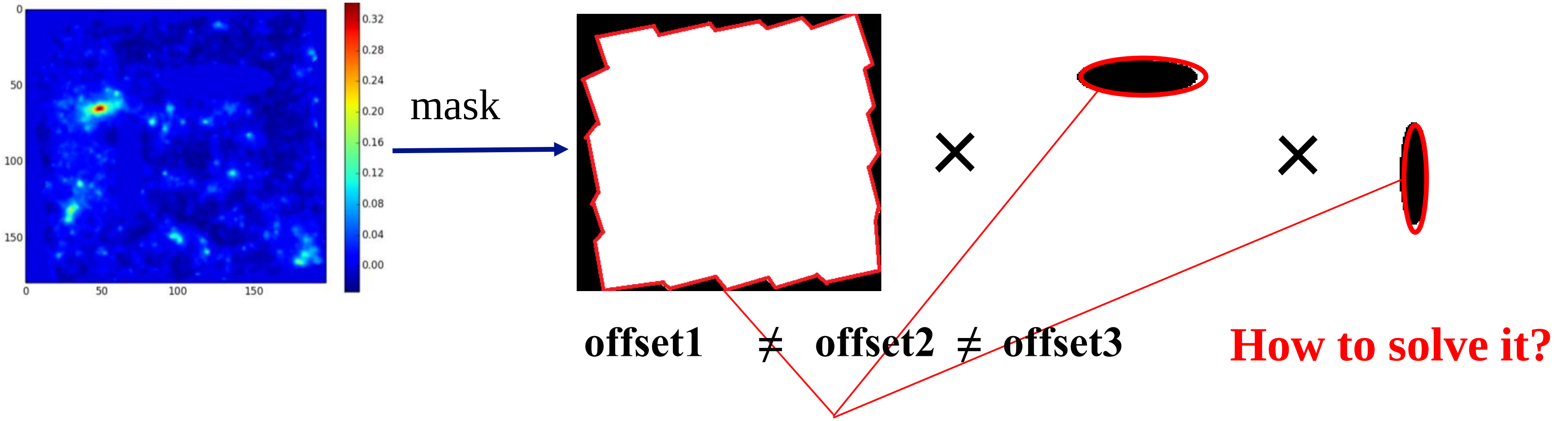

- **Offset problem of the line integral** $\kappa_E = \oint_\Gamma (\boldsymbol{u} - \nabla \times \boldsymbol{\kappa_B}) \cdot d\boldsymbol{s}$

  - The value of the departure point is given arbitrarily. Thus, it is likely to have an offset between the reconstructed dark matter map and the theoretic one.
  - If we compute independently the line integral for each boundary, the offset will be different from one another

Preconstruction – Correction scheme

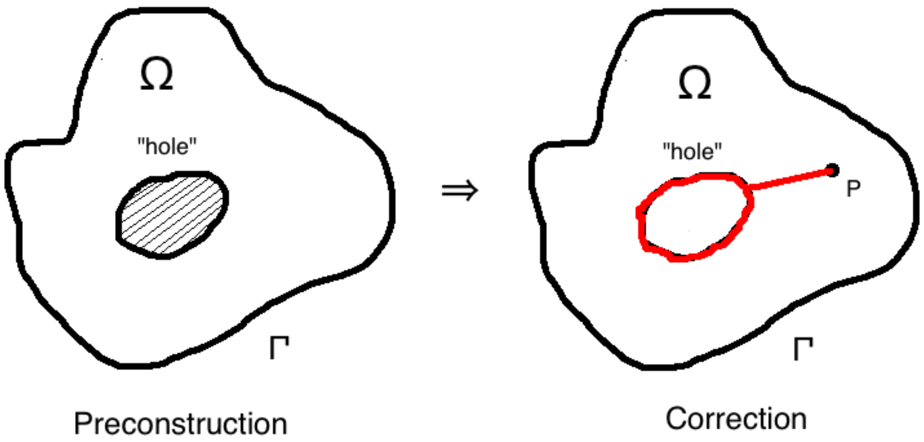

- **Proposal:**

1. Similarly, reconstruct κ_B with the boundary condition $\kappa_B = 0$
2. **Preconstruction.** Reconstruct firstly κ_E with "holes" filled:
   a) Fill each "hole" with average of the edge of the hole
   b) Then, reconstruct κ_E with the outer Dirichlet boundary condition
3. **Correction.** Reconstruct the final κ_E:
   a) Based on κ_E obtained in the step (2), we choose other integral paths to compute the Dirichlet boundary condition for each "hole"
   b) Reconstruct κ_E with all the boundary conditions.

Numerical simulation

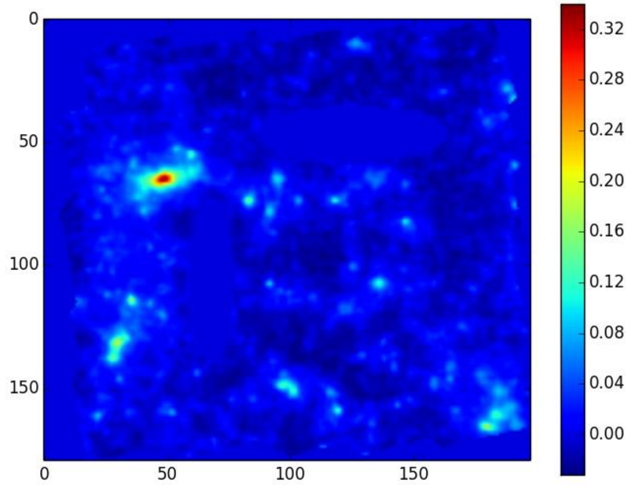

Reconstruction $\tilde{\kappa}_E$

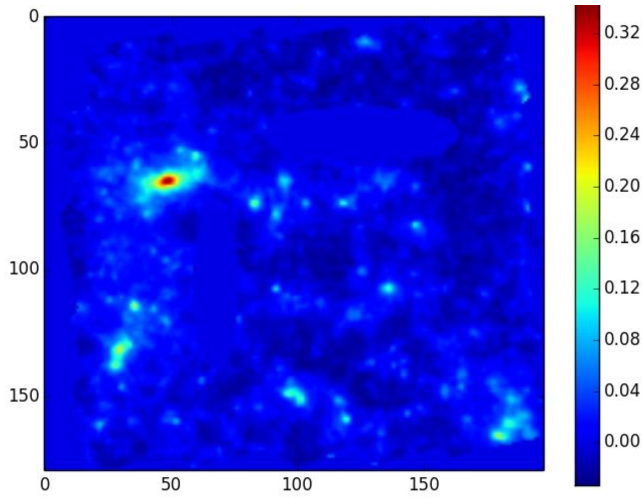

Original κ

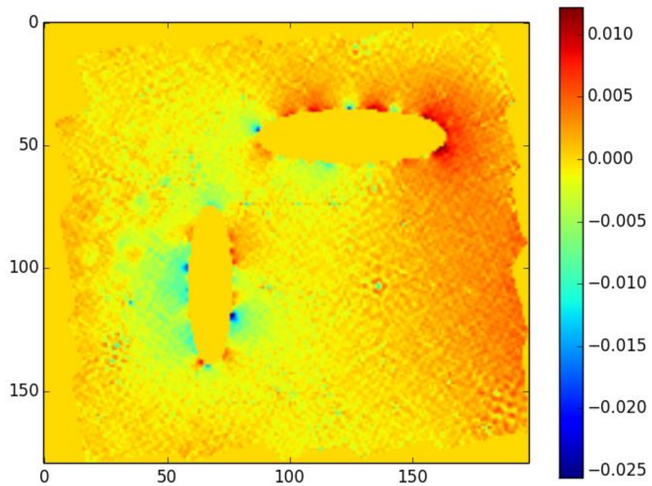

Relative Errors

$$\frac{\left\|\tilde{\kappa}_E - \kappa\right\|_2}{\left\|\kappa\right\|_2} = 9.5\%$$

Dark matter map denoising

Noise robustness of the MG

- **Real data:**
  - $\gamma_n = \gamma + N_b$, where $N_b \sim N\left(\frac{\sigma_\epsilon^\gamma}{\sqrt{N_g}}\right)$, in practice, $N_g \approx 30 \text{ arcmin}^{-2}$, $\sigma_\varepsilon^\gamma \approx 0.3$
- **Noise robustness (MG vs FFT)**

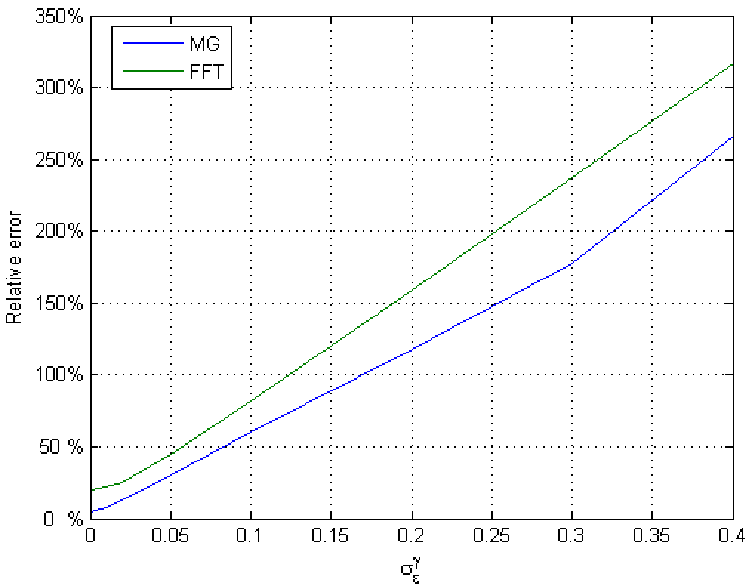

(a)

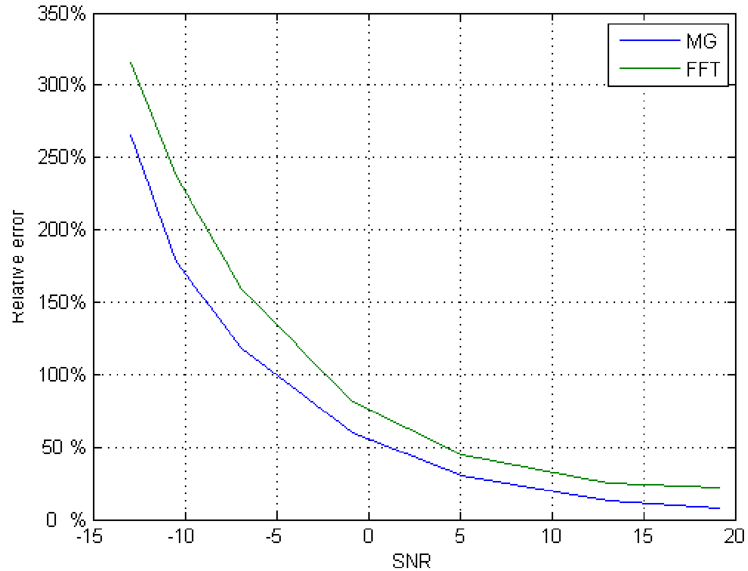

(b)

Figure: The relative error of κ_E versus (a) standard deviation, (b) SNR in dB

Filtering

- **However, using the MG, the noise of $\boldsymbol{\kappa_E}$ is no longer simple Gaussian $\longrightarrow$ Preprocessing of $\boldsymbol{\gamma}$**

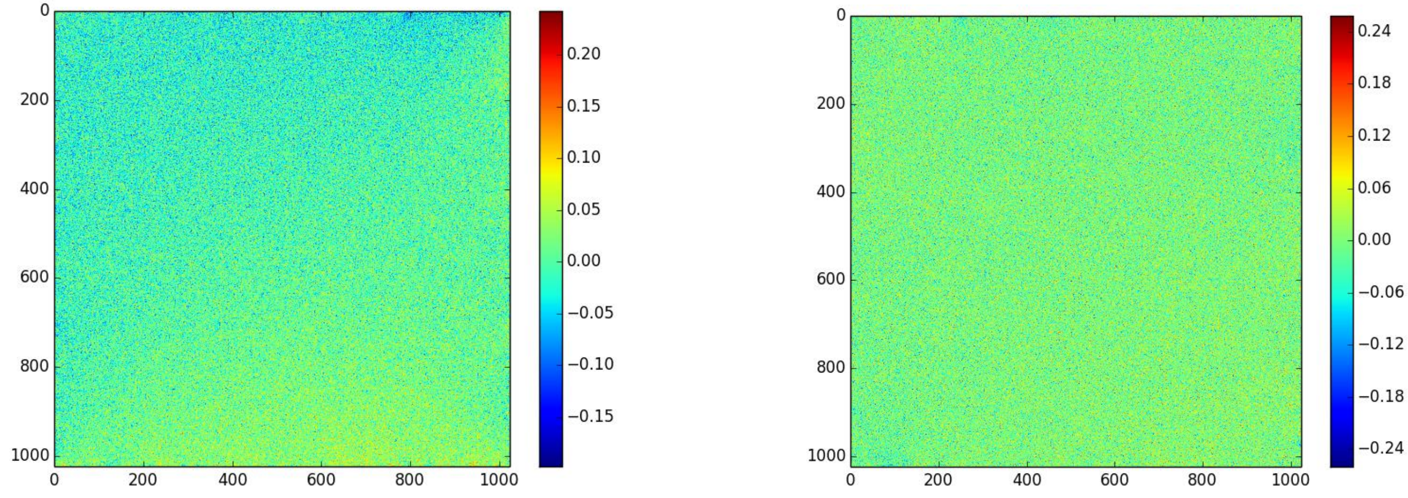

(a) (b)

Figure: Error map between $\tilde{\kappa}_E$ and κ with $\sigma_\epsilon^\gamma = 0.3$: (a) using the MG, (b) using the FFT.

- **Filtering**
  - Linear filters
  - Non-linear filters

Filtering

Linear filters

- Gaussian filter
  - Low pass filter, suppress the high frequencies of the signal

$$\gamma_G = G_\sigma * \gamma_n = G_\sigma * \gamma_{1n} + G_\sigma * \gamma_{2n},$$

where G_σ is a Gaussian function

$$G_\sigma(x, y) = \frac{1}{2\pi\sigma^2} e^{-\frac{(x-x_0)^2+(y-y_0)^2}{2\sigma^2}}$$

It depends strongly on the value of the width σ

- Wiener filter
  - Optimal filter in terms of mean square error for periodic data

$$W(k_1, k_2) = \frac{|\hat{\gamma}(k_1, k_2)|^2}{|\hat{\gamma}(k_1, k_2)|^2 + \left|\hat{N}_b(k_1, k_2)\right|^2}$$

Filtering

Non-linear filters

- Anisotropic filter
  - Perona-Malik filter, nonlinear diffusion for avoiding the blurring and localization problems of linear diffusion filtering.

$$\partial_t \gamma = div(g(|\nabla\gamma|^2)\nabla\gamma),$$

with diffusion function such as

$$\mathrm{g}(\mathrm{s}^2) = \frac{1}{1 + s^2/\lambda^2} \text{ with } \lambda > 0$$

- Wavelet filter
  - Wavelet transform $w = \mathrm{WT}(\gamma_\mathrm{n})$
  - Filtering: threshold t

$$\tilde{w} = \mathrm{HardThresh}(w) = \begin{cases} w & \text{if } |w| \geq t, \\ 0 & \text{otherwise.} \end{cases}$$

Numerical results

Noise level: $\sigma_{\epsilon}^{\gamma} = 0.3$

Theoretic κ

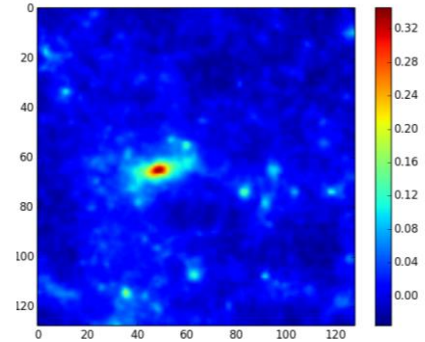

Gaussian filter | Wiener filter | Wavelet filter | Anisotropic filter

MG

FFT

SS

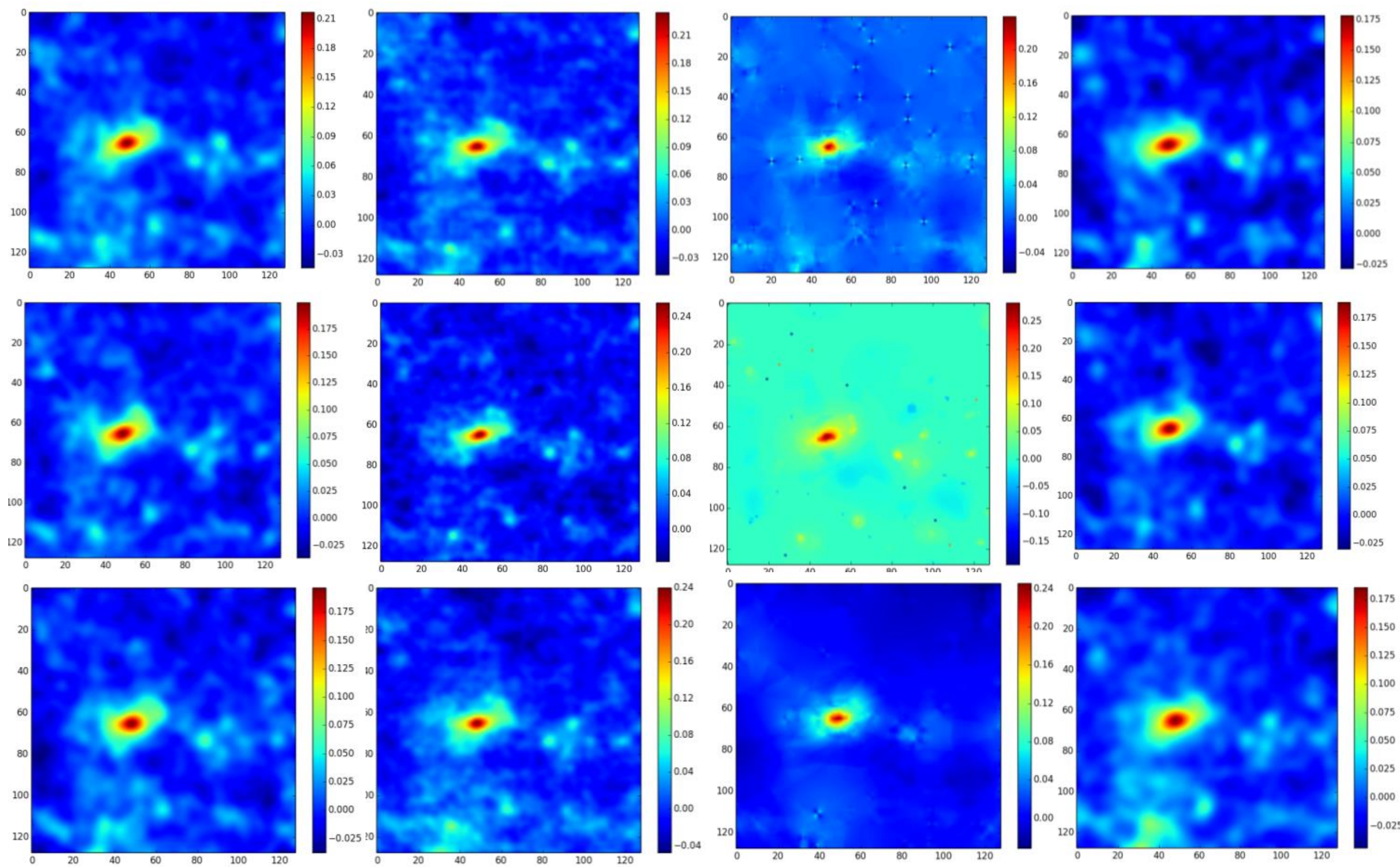

Numerical results

Visual perception

- The performance of the wavelet filter depends on the choice of the representation dictionary
- Anisotropic filter is very close to Gaussian filter as the map is not textured
- Although κ is not Gaussian, Wiener filter gives a reasonable result with a better resolution than Gaussian filter

Quantitatively

- Relative error $\frac{||\tilde{\kappa}_E - \kappa||_2}{||\kappa||_2}$

Filters	MG	FFT	Seitz-Schneider
Gaussian filter	41.5%	46.6%	44.3%
Wiener filter	39.3%	40.5%	44.7%
Wavelet filter	64.6%	61.4%	53.5%
Anisotropic filter	44.9%	47.9%	47.4%

Conclusions

- The MG doesn’t lead to boundary effects compared to the FFT
- The MG is very efficient in solving large-size problem
- The MG integrated by the FDM can be extended to irregular domain, even with absent data inside, valuable in practice to the real telescope survey.
- As for the denoising problem, the preprocessing is considered, and the numerical results prove that Wiener filter gives a better resolution.

Perspectives

- In short term, application to the COSMOS survey
- In long term, denoising problem may be reconsidered using sparse signal processing.

Thank you!

Existing method

- **Fourier Transform:**
  - To remove the partial differential, we transform into Fourier space

$$\begin{cases} \gamma_1 = \frac{1}{2}(\partial_1^2 - \partial_2^2)\psi \\ \gamma_2 = \partial_1 \partial_2 \psi \\ \kappa = \frac{1}{2}(\partial_1^2 + \partial_2^2)\psi \end{cases}$$

  - $\hat{\gamma}_i = \hat{P}_i \hat{k}_i,\ i = 1{,}2$ with $\begin{cases} \hat{P}_1(k) = \frac{k_1^2 - k_2^2}{k_1^2 + k_2^2} \\ \hat{P}_2(k) = \frac{2k_1 k_2}{k_1^2 + k_2^2} \end{cases}$
  - $\hat{\tilde{\kappa}}_n^E = \hat{P}_1 \hat{\gamma}_{1n} + \hat{P}_2 \hat{\gamma}_{2n}$

Multigrid Method (1)

Pseudo-code

Algorithm 1: The MGV scheme algorithm for Poisson's problem $Af = g$

Function f^h = `MGV(`g^h`,`f^h`):`
    if Ω^h = *coarsest grid* **then**
        $f^h = -\frac{1}{4}g^h$;   `/* The factor comes from Laplace operator */`
        return f^h
    else
        $f^h = Relax_{\nu_1}(g^h, f^h)$;
        $r^{2h} = I_h^{2h}(g^h - A^h f^h)$;   `/* Move the residual to` Ω^{2h} `*/`
        $f^{2h} = 0$;   `/* Initial guess of` f^{2h} `*/`
        $f^{2h} = MGV(r^{2h}, f^{2h})$;   `/* Recursion */`
        $f^h = f^h + I_{2h}^h f^{2h}$;   `/* Correction of the solution */`
        $f^h = Relax_{\nu_2}(g^h, f^h)$;
        return f^h
    end
end

Multigrid Method (2)

Restriction

- $R_h^{2h} = restriction\ matrix$
- $R_h^{2h} = \begin{bmatrix} 1/16 & 1/8 & 1/16 \\ 1/8 & 1/4 & 1/8 \\ 1/16 & 1/8 & 1/16 \end{bmatrix}$

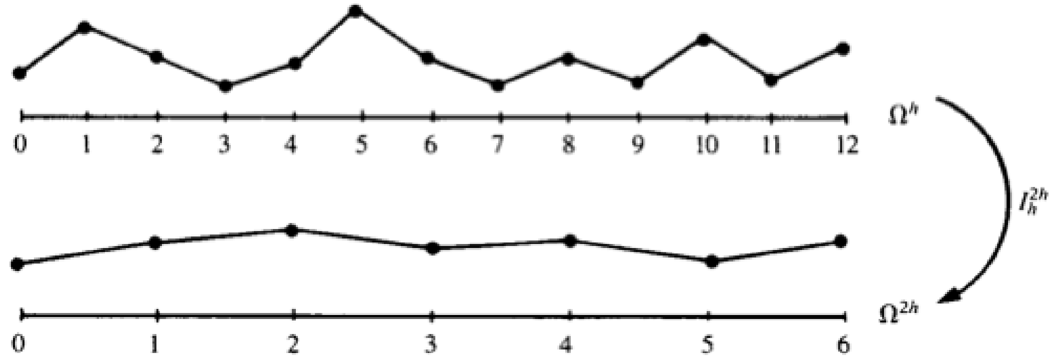

Interpolation

- $I_{2h}^h = interpolation\ matrix$
- $I_{2h}^h = \begin{bmatrix} 1/4 & 1/2 & 1/4 \\ 1/2 & 1 & 1/2 \\ 1/4 & 1/2 & 1/4 \end{bmatrix}$

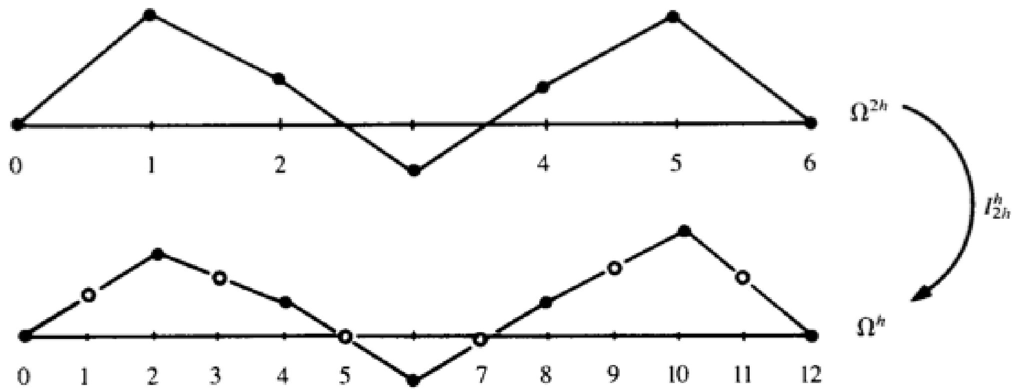

Multigrid Method (3)

- **Restriction model for oblong domain**

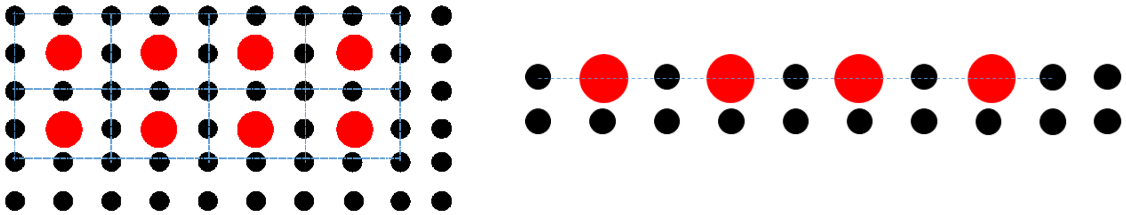

- **Numerical result for oblong domain**

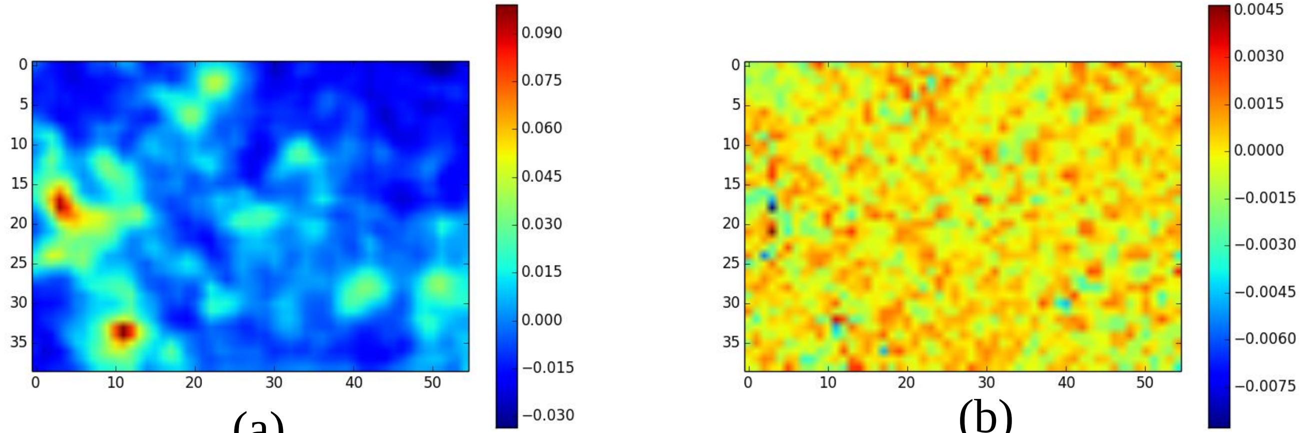

(a) (b)

Figure: (a) Reconstructed dark matter map $\hat{\kappa}_E$ using the MG with 39×55pixels, (b) Error map related to the simulated dark matter map.

Multigrid Method (4)

- **Restriction model for irregular domain**

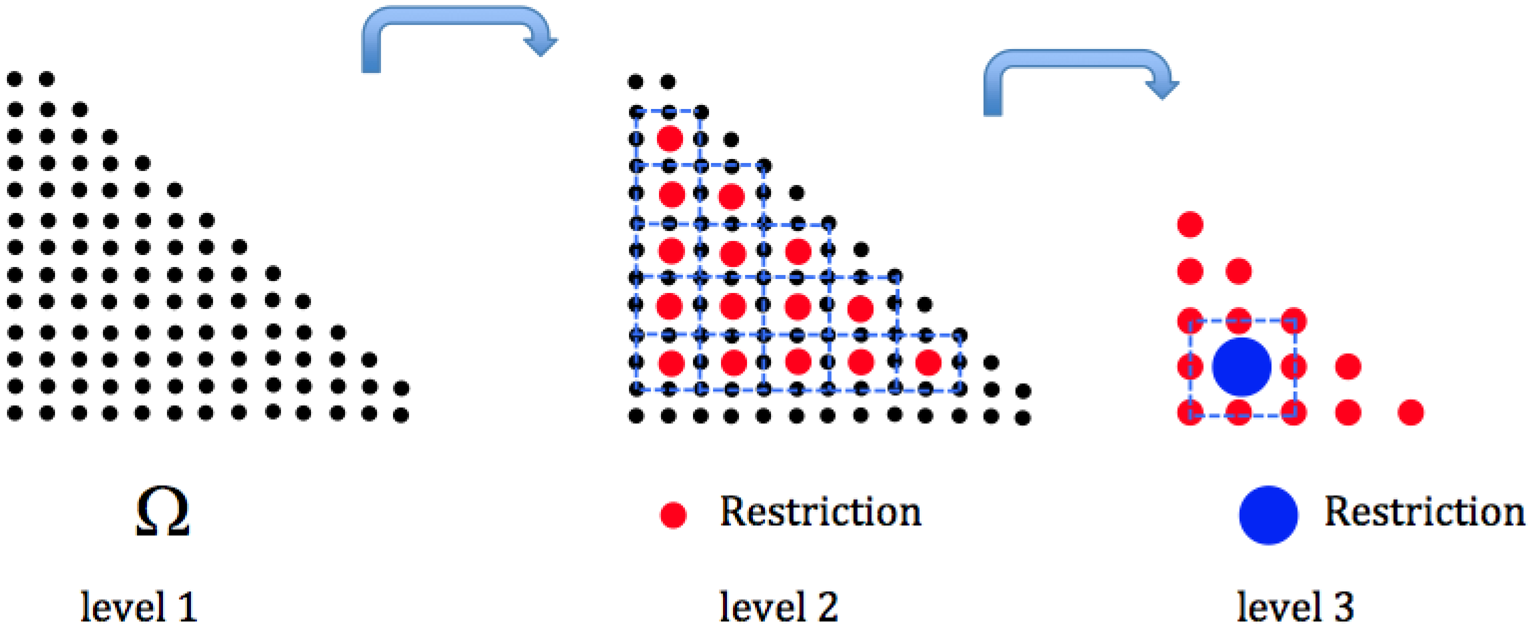

Line integral

- **Model**

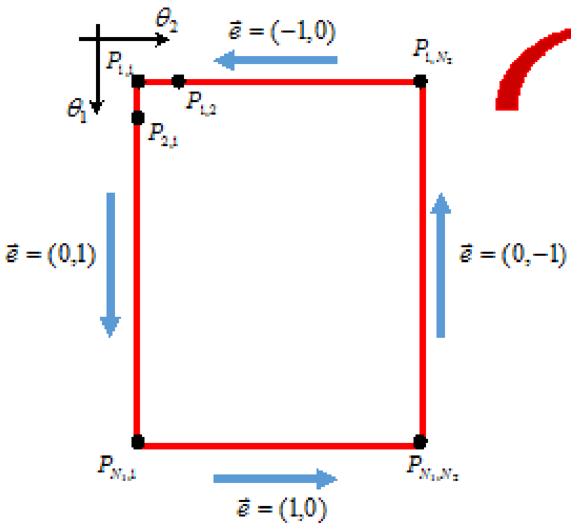

$$\kappa_E = \oint_\Gamma (P de_1 + Q de_2),$$

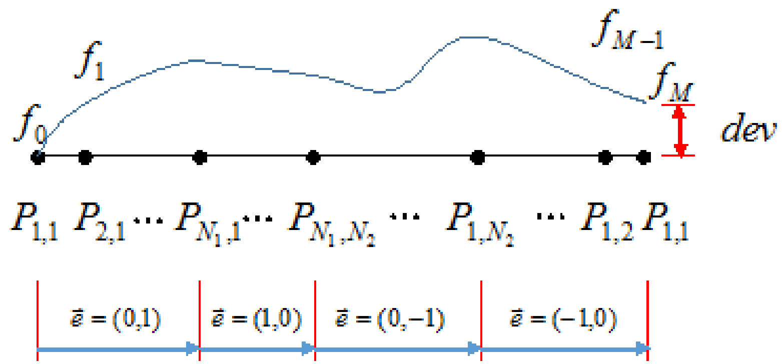

$$f_i = f_{i-1} + \frac{h}{2}(P_i + P_{i+1}), \quad 1 \leqslant i \leqslant M$$

$$\mathbf{e} = (e_1, e_2) = \begin{cases} (0,1) & \text{if } 1 \leqslant \theta_1 \leqslant N_1, \theta_2 = 1, \\ (1,0) & \text{if } \theta_1 = N_1, 1 \leqslant \theta_2 \leqslant N_2, \\ (0,-1) & \text{if } N_1 \geqslant \theta_1 \geqslant 1, \theta_2 = N_2, \\ (-1,0) & \text{if } \theta_1 = 1, N_2 \geqslant \theta_2 \geqslant 1. \end{cases}$$

$$f_i = f_i - \frac{dev}{M-1}(i-1), \quad 1 \leqslant i \leqslant M$$

Anisotropic filter

- **Study of the parameters λ and N**

- The edges are better conserved when λ decreases
- The image is smoother when the smoothing time increases

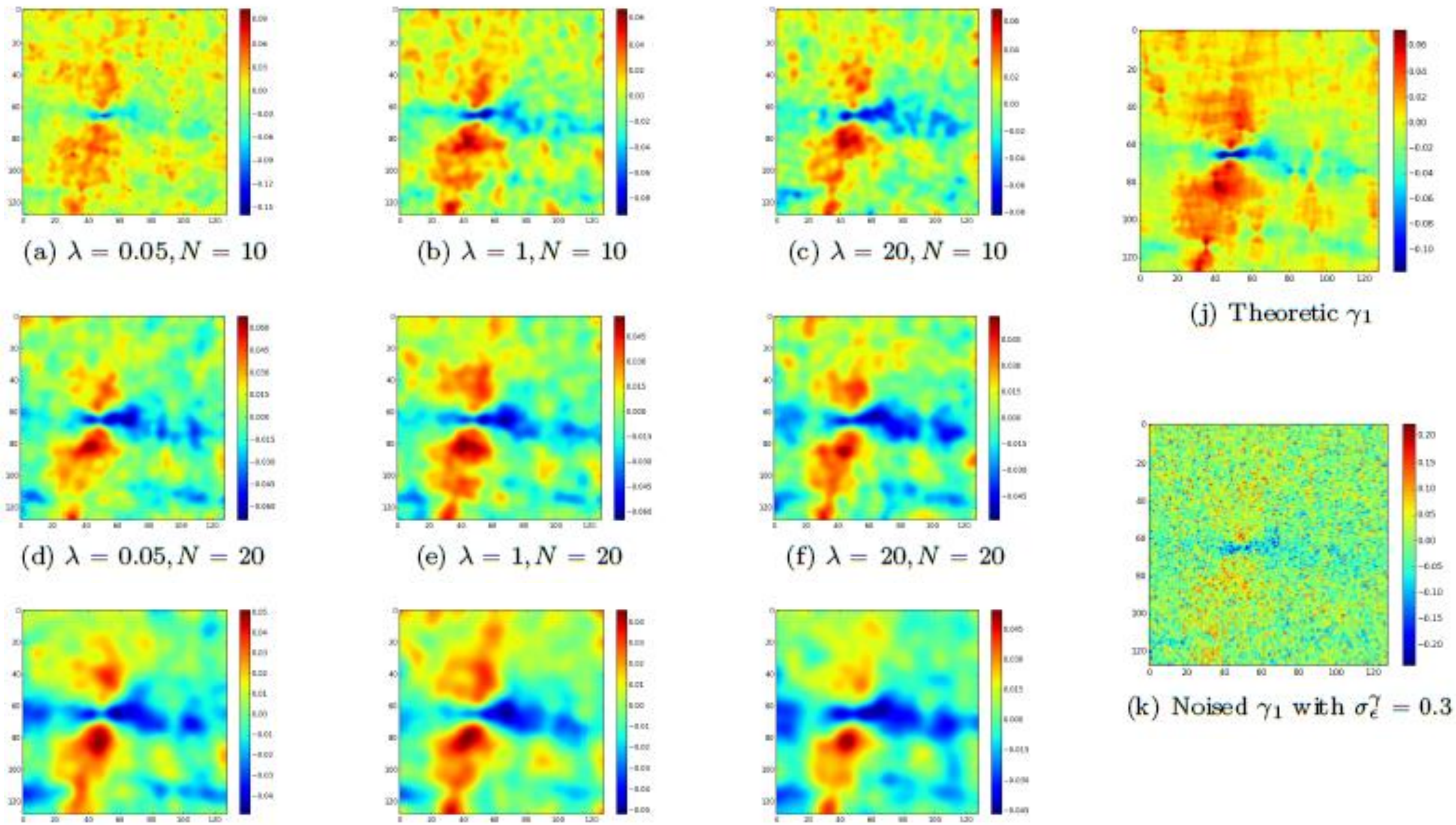

(a) $\lambda = 0.05, N = 10$ (b) $\lambda = 1, N = 10$ (c) $\lambda = 20, N = 10$ (j) Theoretic γ_1

(d) $\lambda = 0.05, N = 20$ (e) $\lambda = 1, N = 20$ (f) $\lambda = 20, N = 20$ (k) Noised γ_1 with $\sigma_\epsilon^\gamma = 0.3$

(g) $\lambda = 0.05, N = 40$ (h) $\lambda = 1, N = 40$ (i) $\lambda = 20, N = 40$

Gaussian filter

- **Study of Gaussian width σ**
  - the relative error firstly drops rapidly and then rises very slowly. We can easily find out the optimal Gaussian width $\sigma = 2 \sim 3$ for the filter.